Communication

A Novel Thermodynamic Model for Obtaining Solid–Liquid Interfacial Energies

CONG ZHANG and YONG DU

The modeling of solid–liquid interfacial energies is developed in the present work. The total interfacial energy is separated into chemical and structure contributions, which are estimated by applying reported Gibbs energies, as well as correlated with molar interfacial area and melting temperature of solid phase. The present model is well validated with comprehensive datasets of measured solid–liquid interfacial energies, and it can provide key input parameters for microstructure simulations.

DOI: 10.1007/s11661-017-4365-6

Solid–liquid interfacial energy is a thermophysical property that describes the interfacial state between the solid and liquid phases. It plays an important role in various material science phenomena, such as nucleation, wetting, and adsorption. In addition, the morphology and growth kinetics of dendrites during directional solidification,[1,2] dissolution and precipitation rate during semi-solid processing,[3] as well as grain growth behavior during liquid-phase sintering of cermets and cemented carbides[4–6] are greatly influenced by interfacial energy. Experimental determination of this property involves complex procedures, while the number of valuable solid–liquid combinations to test is immense. Models to obtain solid–liquid interfacial energies through theoretical derivations is therefore of great value.

A comprehensive review of models describing solid–liquid interfacial energies, on the basis of thermodynamic considerations, was presented by Lippmann *et al.*[7] In that paper,[7] Benedictus' model[8] regarding the temperature and concentration dependence of enthalpy and entropy quantities *via* CALPHAD (CALculation of PHAse Diagrams) approach was modified. The interfacial energy between solid and liquid phases with equilibrium atomic compositions is closely related to chemical potentials (partial molar Gibbs free energies) of each component, so it is natural to extract solid–liquid interfacial energies from bulk Gibbs energies, as was reasonably achieved in the modeling work by Warren.[9] In Warren's model, the solid–liquid interface was treated as an ideal plane with two atomic layers: one layer for the liquid state and the other for the solid. The total interfacial energy was separated into chemical and structure contributions, which were correlated with molar Gibbs energy of the system and solid–liquid interfacial energy of the solid phase, respectively. According to Warren,[9] the Gibbs energy curves of solid and liquid phases were mathematically fitted based on the melting temperatures of pure components and published phase equilibria. However, with the development of the CALPHAD technique, it is more accurate to find Gibbs energies through thermodynamic evaluations. Generally, the particle geometry in an equilibrium solid–liquid system tends to be spherical if the anisotropy of crystal structure is not apparent. Therefore, it should be an improvement if the solid–liquid interface is described as a sphere. Due to the inappropriate description of the Gibbs energy and interfacial geometry, the Warren model is further developed to obtain a better estimation of solid–liquid interfacial energies.

In a hypothetical binary A–B system, the liquid (L) and solid (S) phases are thermodynamically stable within specific temperature and composition ranges. The solid–liquid interface is assumed to contain two atomic layers with no concentration gradient, which leads to the liquid and solid layers having identical compositions of their corresponding bulk phases. The Gibbs free energies of (L) and (S) states are schematically presented in Figure 1, and the compositions of the liquid (x_1) and solid (x_2) phases are defined by the common tangent. The effective composition of the interface is defined as x_i, and is located between the bulk equilibrium compositions x_1 and x_2. The excess free energy of this non-equilibrium composition over that of the bulk solid and liquid states is taken as the contribution of interfacial energy.

The interfacial energy (γ_{SL}) was modeled as separated parts of chemical ($\gamma_{SL(c)}$) and structure ($\gamma_{SL(B)}$) contributions by Warren,[9] which is also followed in the present work:

$$\gamma_{SL} = \gamma_{SL(c)} + \gamma_{SL(B)}. \quad [1]$$

The chemical contribution of the interface atoms to the interfacial energy is generated between the equilibrium molar free energy (G_1) of the atoms in an

CONG ZHANG is with the Collaborative Innovation Center of Steel Technology, University of Science and Technology Beijing, Beijing 100083, People's Republic of China and also with State Key Laboratory of Powder Metallurgy, Central South University, Hunan 410083, People's Republic of China. YONG DU is with the State Key Laboratory of Powder Metallurgy, Central South University. Contact e-mail: yong-du@csu.edu.cn

Manuscript submitted April 14, 2017.
Article published online October 6, 2017

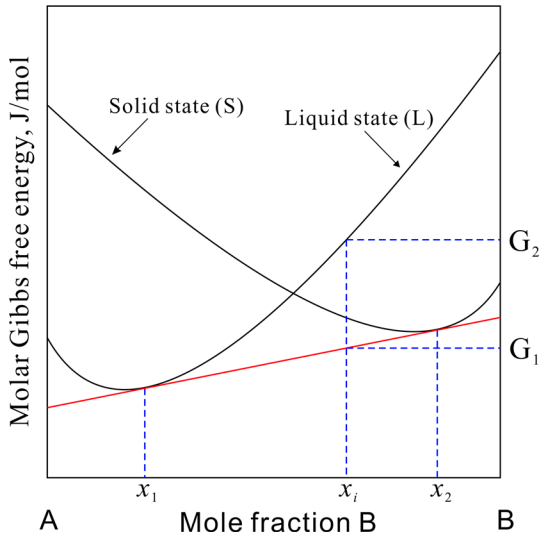

Fig. 1—Molar Gibbs free energy curves of A–B system, where L is liquid phase and S is solid phase.

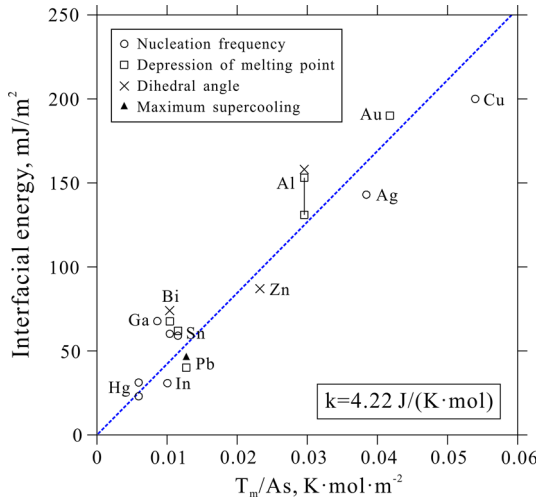

Fig. 2—Linear fitting of Eq. [7] for the structure contribution. The solid–liquid interfacial energies of pure metals based on different measurement techniques are taken from the review work by Eustathopoulos.[13]

equilibrium two-phase mixture and their energy (G_2) when forced to exist together as a liquid of composition x_i. The above assumption makes it possible to write the chemical contribution as follows:

$$\gamma_{SL(c)} = (G_2 - G_1)/A_m, \quad [2]$$

where A_m is the interfacial area per mole of interface atoms. As the interface is constructed by solid and liquid layers, obtaining the effective interfacial composition (x_i) and molar interfacial area of solid and liquid phases is the key to solving Eq. [2].

The molar interfacial area of individual phases is defined as

$$A_i = A_{S/L}/n_A \quad [3]$$

in which n_A is the mole of interface atoms for one layer of phase i, $A_{S/L}$ is the total area of the solid–liquid interface, and i stands for solid ($i = S$) or liquid ($i = L$) state. For a monolayer of phase i with a spherical shape, its molar interfacial area has been deduced by Kaptay[10] as

$$A_L = (\pi/6)^{1/3} \cdot V_L^{2/3} \cdot N_A^{1/3} \quad [4a]$$

$$A_S = (\pi/6)^{1/3} \cdot V_S^{2/3} \cdot N_A^{1/3}, \quad [4b]$$

where N_A is the Avogadro's number, V_i $(i = L, S)$ is the molar volume of the bulk phase, and $(\pi/6)^{1/3} = 0.806$ is a constant for the interface with a spherical geometry. Therefore, the effective composition of the interface in terms of B atom concentration can be expressed as follows:

$$x_i = [(1/A_L) \cdot x_1 + (1/A_S) \cdot x_2]/[(1/A_L) + (1/A_S)] \quad [5]$$

in which $1/A_L$ and $1/A_S$ are the mole amount of liquid and solid components per unit of area, respectively.

Recalling the knowledge that the interface contains the same area of solid and liquid monolayers, the interfacial area per mole of atoms can be determined as

$$A_m = 1/[(1/A_L) + (1/A_S)]. \quad [6]$$

Combining Eqs. [2] to [6] provides the chemical contribution of the solid–liquid interfacial energy. The calculations involved with thermodynamic Gibbs energies were performed based on Thermo-Calc software.[11]

The structure contribution is considered equal to the interfacial energy between the pure solid phase and its melt. Its correlation with melting temperature and molar interfacial area of solid phase is preferred[12]:

$$\gamma_{SL(B)} = k \cdot T_m/A_S, \quad [7]$$

where T_m is the melting temperature of solid phase, and k is an empirical constant. Based on the reported solid–liquid interfacial energies,[13] melting temperatures,[14] crystallographic information,[15] as well as molar volume of liquid[16,17] for pure metals, the linear fitting of Eq. [7] can be achieved for $k = 4.22\ J \cdot K^{-1} \cdot mol^{-1}$, as presented in Figure 2.

The model proposed in Eqs. [1] to [7] has been utilized to estimate the solid–liquid interfacial energies of binary alloys. The results are shown in Figure 3(a) in comparison with experimental datasets[13,18,19] and the predictions by Warren.[9] The thermodynamic parameters reported in the literature were adopted for Al-Sn,[20] Cu-Pb,[21] Sn-Zn,[22] Ag-Pb,[23] Cu-Fe,[24] Cu-Nb,[25] and Fe-Pb[26] systems. It is shown in Figure 3(a) that most of the experimental data are well reproduced by the present model considering the expected experimental uncertainties. The temperature dependence of interfacial energies for Cu-Fe, Cu-Pb, and Fe-Pb alloys are predicted reasonably. Moreover, this model yields a better estimate than Warren's model. Since the Gibbs energies of

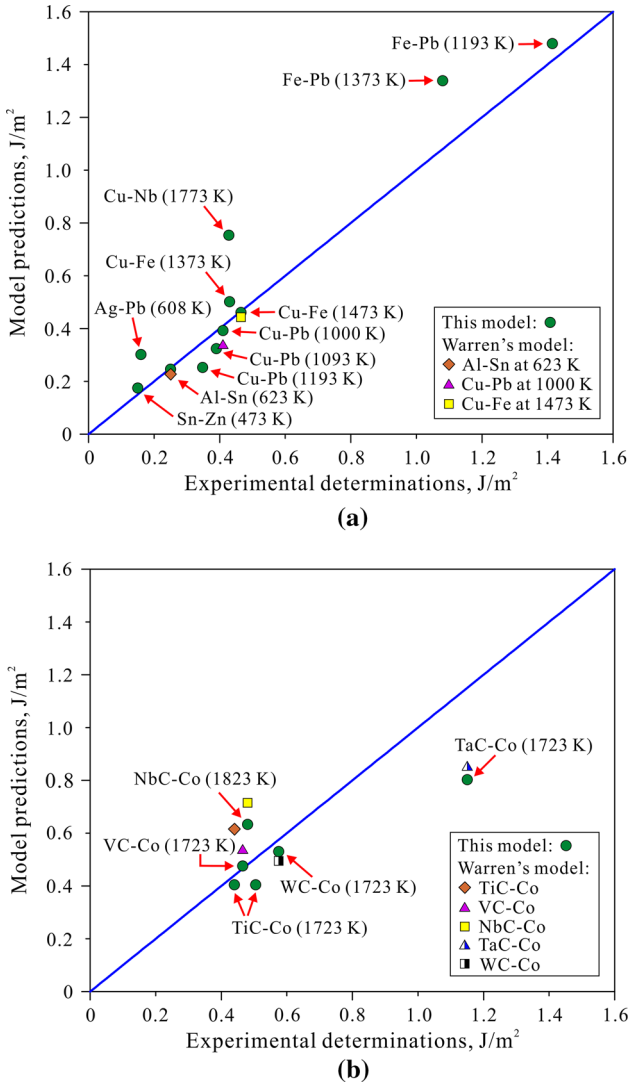

Fig. 3—Comparison of the solid–liquid interfacial energies of (*a*) binary and (*b*) pseudo-binary carbide systems between the predicted values by the present model and the experimental data.[13,18,19,27,28] The estimates from Warren's model[9] are also attached.

bulk alloys have a large influence on the calculated interfacial energies, some of the published interfacial energies for binary alloys cannot be predicted due to the lack of reliable thermodynamic descriptions, such as Ag-Cr, Ag-Fe, Cu-W, Mo-Sn, and Sn-W systems.

In many multicomponent systems, the liquid phase can exist in equilibrium with a stable solid compound such that their phase relationships can be described by a pseudo-binary phase diagram. The present model can be extended to such systems if it is assumed that the compound retains its stoichiometry and its molecules are treated as single species. The calculated solid–liquid interfacial energies for WC-Co, TiC-Co, TaC-Co, VC-Co, and NbC-Co alloys are presented in Figure 3(b), together with the experimental data by Warren and Waldron[27,28] as well as the predictions by Warren's model.[9] In the calculations, the thermodynamic descriptions of these ternary systems[29] were applied, and pseudo-binary lines can be defined in the isothermal sections to find the equilibrium compositions. As depicted in Figure 3(b), the present model shows a better overall agreement with the experimental results than Warren's model, which verifies the rationality of this approach. It is noticeable that the calculated interfacial energy for TaC-Co system is not in better agreement compared with Warren's model, which is due to large discrepancy between the calculated and measured values, and can be ascribed to the following reasons. According to the experimental work by Warren,[27] the solid–liquid interfacial energy of TaC-Co alloy shows obvious anisotropy, thus large error cannot be avoided when determining the interfacial energy. On the other hand, the reported phase equilibria for C-Co-Ta system are not plentiful enough to assess the precise Gibbs energies, which in turn affect the accurate calculation of interfacial energy for TaC-Co system.

To clarify the separate contributions of spherical interface modification and the use of Thermo-Calc Gibbs energies in the present model, the calculations of interfacial energies by means of Warren's model (plan interfaces) applying Thermo-Calc Gibbs energies are performed. The calculated results are listed in Table I, together with solid–liquid interfacial energies from Warren's model, this model, and experimental work. According to this table, the spherical interface modification shows notable improvement compared with plan interface treatment. Moreover, the optimal predictions of interfacial energies cannot be revealed by using only Thermo-Calc Gibbs energies, because the introduction of spherical geometry for interfaces and the utilization of CALPHAD techniques are indispensable parts for the improvements of this model.

The extended application of the present model is to provide a parameter input for microstructure simulation, with an important case being the grain growth simulation of cermets during liquid-phase sintering. Cermets are hard materials that consist of refractory hard phases embedded in ductile binder metals, and are used extensively in cutting tools. The control of grain size is an important aspect of cermet production, as it strongly affects the mechanical properties and cutting performance. The grain growth of carbides during liquid-phase sintering is dominated by Ostwald ripening, for which the driving force is related to the total solid–liquid interfacial energy. This kind of simulation can be accomplished with the help of TC-PRISMA software,[30] as long as the thermodynamic, kinetic, molar volume, and interfacial energy data are provided.

The grain growth behavior of TiC containing 20 vol pct Co during liquid-phase sintering at 1723 K, 1773 K, and 1823 K (1450 °C, 1500 °C, and 1550 °C) was investigated by Warren and Waldron.[31] The carbide grain size was measured by the mean linear intercepts ($\bar{d}$) in combination with optical micrographs of the sintered body. Since the TiC particles are close to being spherical, the intercepts were placed randomly for the measurement. The mean intercept of TiC particles can be transformed into equivalent circle radius (r_c) by the following relationship:

Table I. Calculated Solid–Liquid Interfacial Energies of Binary Alloys and Metal-Carbide Systems in Comparison with Warren's Model and Experimental Investigations*

System	Temperature	Model (P)**	Model (S)†	Warren's model	Experimental data
Al-Sn	623 K (350 °C)	0.199	0.247	0.227	0.250[13]
Cu-Pb	1000 K (727 °C)	0.316	0.392	0.339	0.410[18]
	1093 K (820 °C)	0.261	0.324	—	0.390[13]
	1193 K (920 °C)	0.204	0.253	—	0.348[13]
Sn-Zn	473 K (200 °C)	0.141	0.175	—	0.150[13]
Ag-Pb	608 K (335 °C)	0.243	0.302	—	0.160[13]
Cu-Fe	1373 K (1100 °C)	0.405	0.502	—	0.430[13]
	1473 K (1200 °C)	0.373	0.463	0.443	0.465[19]
Cu-Nb	1773 K (1500 °C)	0.608	0.754	—	0.428[13]
Fe-Pb	1193 K (920 °C)	1.193	1.480	—	1.415[13]
	1373 K (1100 °C)	1.079	1.339	—	1.080[13]
WC-Co	1723 K (1450 °C)	0.428	0.531	0.495	> 0.575[27]
TiC-Co	1723 K (1450 °C)	0.326	0.405	0.615	0.440[28], 0.505[27]
TaC-Co	1723 K (1450 °C)	0.647	0.803	0.855	1.150[27]
VC-Co	1723 K (1450 °C)	0.384	0.476	0.540	0.465[28]
NbC-Co	1823 K (1550 °C)	0.510	0.633	0.715	0.480[28]

*The unit of interfacial energies in this table is J/m^2.
**Model (P) applies plane geometry of interfaces and Thermo-Calc Gibbs energies.
†Model (S) applies spherical geometry of interfaces and Thermo-Calc Gibbs energies, which is the model developed in this work.

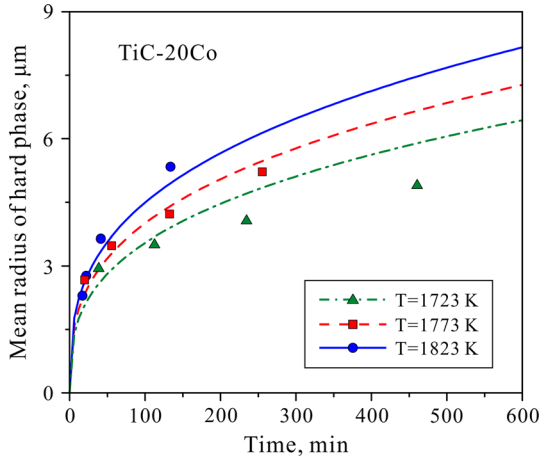

Fig. 4—The TC-PRISMA simulated grain growth behavior of hard phase in TiC-20 vol pct Co alloy sintered at 1723 K, 1773 K, and 1823 K (1450 °C, 1500 °C, and 1550 °C). The solid–liquid interfacial energies were obtained according to the present model, while the grain growth experimental data were reported by Warren and Waldron.[31]

$$\overline{d} = (\pi \cdot r_c)/2. \quad [8]$$

Figure 4 displays the simulated results for the average grain size of the TiC-based cermet containing 20 vol pct Co during isothermal holding. The thermodynamic and kinetic databases[29,32] as well as molar volume data[15–17] for TiC and liquid phases were employed. The solid–liquid interfacial energies between TiC and liquid Co were estimated, according to the present model, to be 0.405 J/m^2 at 1723 K (1450 °C), 0.407 J/m^2 at 1773 K (1500 °C), and 0.428 J/m^2 at 1823 K (1550 °C), respectively. It is shown in Figure 4 that the grain growth of TiC phase is enhanced at high temperatures. As the growth of hard phase is realized through diffusion transport of liquid during the continuous process of dissolution and precipitation, and the high temperature provides higher diffusivity in the liquid phase. The high diffusion rate and interfacial energy (driving force) are responsible for the favorable grain growth at high temperatures. By comparing the results of simulations and experiments in Figure 4, it is found that the simulated results at 1773 K and 1823 K (1500 °C and 1550 °C) are in good agreement with the experiments. However, the simulation at 1723 K (1450 °C) is somewhat higher than the experimental determinations. This is due to the fact that the decrease in temperature will lower the volume fraction of liquid phase, leading to an increase of contiguity between hard phases, which can retard the hard phases from growing significantly.[33]

In summary, a novel thermodynamic model of solid–liquid interfacial energies is developed in this work. The introduction of spherical geometry for interfaces together with the utilization of CALPHAD techniques are significant improvements. This model can be extended to multicomponent systems provided that it is simplified as a pseudo-binary system. The present model is well validated by comprehensive datasets of reported solid–liquid interfacial energies for various alloys and metal carbides. Furthermore, microstructure simulations can be performed with key input parameters obtained using this model, such as grain growth simulations during liquid-phase sintering.

The financial supports from the National Natural Science Foundation of China (Grant Nos. 51371199 and 51701013) and Ministry of Industry and Information Technology of China (Grant No. 2015ZX04005008) are greatly acknowledged. The authors thank Dr. Qing

Chen at Thermo-Calc Software AB of Sweden for valuable discussions.

REFERENCES

1. J. Choi, S.-K. Park, H.-Y. Hwang, and J.-Y. Huh: *Acta Mater.*, 2015, vol. 84, pp. 55–64.
2. A. Viardin, M. Zaloznik, Y. Souhar, M. Apel, and H. Combeau: *Acta Mater.*, 2017, vol. 122, pp. 386–99.
3. T. Nagira, S. Morita, H. Yokota, H. Yasuda, C.M. Gourlay, M. Yoshiya, A. Sugiyama, K. Uesugi, A. Takeuchi, and Y. Suzuki: *Metall. Mater. Trans. A*, 2014, vol. 45A, pp. 5613–23.
4. K.S. Vinod: *Comprehensive Hard Materials*, 1st ed., Elsevier Press, Oxford, 2014.
5. C. Zhang, Y. Du, S. Zhou, Y. Peng, and J. Wang: *Ceram. Int.*, 2016, vol. 42, pp. 19289–95.
6. J. Long, W. Zhang, Y. Wang, Y. Du, Z. Zhang, B. Lu, K. Cheng, and Y. Peng: *Scr. Mater.*, 2017, vol. 126, pp. 33–36.
7. S. Lippmann, I.-H. Jung, M. Paliwal, and M. Rettenmayr: *Philos. Mag.*, 2016, vol. 96, pp. 1–14.
8. R. Benedictus, A. Bottger, and E.J. Mittemeijer: *Phys. Rev. B*, 1996, vol. 54, pp. 9109–25.
9. R. Warren: *J. Mater. Sci.*, 1980, vol. 15, pp. 2489–96.
10. G. Kaptay: *Acta Mater.*, 2012, vol. 60, pp. 6804–13.
11. B. Sundman, B. Jansson, and J.O. Andersson: *CALPHAD*, 1985, vol. 9, pp. 153–90.
12. G. Grimvall and S. Sjodin: *Phys. Scr.*, 1974, vol. 10, pp. 340–52.
13. N. Eustathopoulos: *Int. Met. Rev.*, 1983, vol. 28, pp. 189–210.
14. A.T. Dinsdale: *CALPHAD*, 1991, vol. 15, pp. 317–425.
15. http://crystdb.nims.go.jp/.
16. T. Iida and R.I.L. Guthrie: *The Physical Properties of Liquid Metals*, 1st ed., Oxford University Press, New York, 1988.
17. A.I. Savvatimskiy: *J. Phys. Condens. Matter*, 2008, vol. 20, p. 114112.
18. N. Eustathopoulos, L. Coudurier, J.C. Joud, and P. Desre: *J. Chim. Phys. Phys.-Chim. Biol.*, 1974, vol. 71, pp. 1465–71.
19. Y.N. Levin and G.I. Ivantsov: *Fiz. Met. Metalloved.*, 1963, vol. 16, pp. 535–39.
20. I. Ansara: *COST 507-Thermochemical Database for Light Metal Alloys*, European Commission, Brussels/Luxembourg, 1995.
21. B. Onderka and L.A. Zabdyr: *Scand. J. Metall.*, 2001, vol. 30, pp. 320–23.
22. H. Ohtani, M. Miyashita, and K. Ishida: *J. Japan Inst. Metals*, 1999, vol. 63, pp. 685–94.
23. B.-Z. Lee, C.-S. Oh, and D.N. Lee: *J. Alloys Compd.*, 1994, vol. 215, pp. 293–301.
24. M.A. Turchanin, P.G. Agraval, and I.V. Nikolaenko: *J. Phase Equilib.*, 2003, vol. 24, pp. 307–19.
25. M. Hamalainen, K. Jaaskelainen, R. Luoma, M. Nuotio, P. Taskinen, and O. Teppo: *CALPHAD*, 1990, vol. 14, pp. 125–37.
26. I. Vaajamo and P. Taskinen: *Thermochim. Acta*, 2011, vol. 524, pp. 56–61.
27. R. Warren: *Metallography*, 1976, vol. 9, pp. 183–91.
28. R. Warren and M.B. Waldron: *Nat. (London) Phys. Sci.*, 1972, vol. 235, pp. 73–74.
29. Y. Peng, Y. Du, P. Zhou, W. Zhang, W. Chen, L. Chen, S. Wang, G. Wen, and W. Xie: *Int. J. Refract. Met. Hard Mater.*, 2014, vol. 42, pp. 57–70.
30. Q. Chen, H.J. Jou, and G. Sterner: *TC-PRISMA User's Guide and Examples*, Thermo-Calc Software AB, Stockholm, 2011.
31. R. Warren and M.B. Waldron: *Powder Met.*, 1972, vol. 15, pp. 180–201.
32. W. Zhang, Y. Du, W. Chen, Y. Peng, P. Zhou, S. Wang, G. Wen, and W. Xie: *Int. J. Refract. Met. Hard Mater.*, 2014, vol. 43, pp. 164–80.
33. M. Pellan, S. Lay, J.-M. Missiaen, S. Norgren, J. Angseryd, E. Coronel, and T. Persson: *J. Am. Ceram. Soc.*, 2015, vol. 98, pp. 3596–3601.